NUMERICAL TREATMENT OF TWO-PHASE FLOW IN CAPILLARY HETEROGENEOUS POROUS MEDIA BY FINITE-VOLUME APPROXIMATIONS

HELMER ANDRÉ FRIIS[A] AND STEINAR EVJE[B,C]

Abstract. This paper examines two-phase flow in porous media with heterogeneous capillary pressure functions. This problem has received very little attention in the literature, and constitutes a challenge for numerical discretization, since saturation discontinuities arise at the interface between the different homogeneous regions in the domain. As a motivation we first consider a one-dimensional model problem, for which a semi-analytical solution is known, and examine some different finite-volume approximations. A standard scheme based on harmonic averaging of the absolute permeability, and which possesses the important property of being pressure continuous at the discrete level, is found to converge and gives the best numerical results. In order to investigate two-dimensional flow phenomena by a robust and accurate numerical scheme, a recent multi point flux approximation scheme, which is also pressure continuous at the discrete level, is then extended to account for two-phase flow, and is used to discretize the two-phase flow pressure equation in a fractional flow formulation well suited for capillary heterogenity. The corresponding saturation equation is discretized by a second-order central upwind scheme. Some numerical examples are presented in order to illustrate the significance of capillary pressure heterogeneity in two-dimensional two-phase flow, using both structured quadrilateral and unstructured triangular grids.

AMS Subject Classifications: 65M60, 76S05, 35R05

Key words. two-phase flow, heterogeneous media, capillary pressure, finite volume, MPFA, unstructured grids

1. Introduction

The study of two-phase flow in porous media has significant applications in areas such as hydrology and petroleum reservoir engineering. The flow pattern is mainly governed by the geometric distribution of absolute permeability, which may be anisotropic and highly heterogeneous, the form of the relative permeability and capillary pressure functions and gravity [4]. The corresponding system of partial differential equations describing the flow consists of an elliptic and an essentially hyperbolic part, usually denoted the pressure- and saturation equation, respectively. This system is rather challenging, and quite a lot of research has been devoted to its solution during the last decades.

In recent years several discretization methods that can treat unstructured grids in combination with discontinuous and anisotropic permeability fields have been developed for the elliptic pressure equation. Important examples are the flux-continuous finite volume schemes introduced in e.g. [11, 12, 25, 13, 15, 5, 6], which have been termed multi point flux approximation methods (MPFA) schemes, and the mixed finite element (MFE) and related schemes, e.g., [1, 2, 9, 20, 18]. The MFE and related methods solve for both control-volume pressure and cell face velocities leading to a globally coupled indefinite linear system (saddle point problem), while the more efficient MPFA methods only solve for control-volume pressure and have a locally coupled algebraic system for the fluxes that yield a consistent continuous approximation, while only requiring one third the

Date: April 6, 2011.

[A]International Research Institute of Stavanger, P.O.Box 8046, 4068 Stavanger, Norway.
[B]University of Stavanger, 4036 Stavanger, Norway.
Email: HelmerAndre.Friis@iris.no, Steinar.Evje@uis.no.
[C]Corresponding author.

number of degrees of freedom of the mixed method when compared on a structured grid (and a quarter in three dimensions). The latter methods are clearly advantageous, particularly for time-dependent problems, as the extra degrees of freedom required by the mixed method add further computational complexity and a severe penalty to simulation costs. For the saturation equation some higher order schemes have been employed, as well as various types of so called fast tracking schemes, but the standard first order upwind scheme is still widely used in commercial simulators.

However, the main body of research literature devoted to two-phase flow in porous media concerns flow in the absence of capillary pressure, or assumes a homogeneous capillary pressure function in the domain. Obviously, there are a number of flow cases for which these assumptions are valid, but this observation is nevertheless noticeable since heterogeneity in capillary pressure may often have a significant effect on the flow pattern, and in certain cases it can be as important as absolute permeability heterogeneity [19].

From the very sparse literature devoted to capillary pressure heterogeneity in porous media, we would like to mention the work of Yortsos and Chang [27]. They studied analytically the capillary effect in steady-state flow in one-dimensional (1D) porous media. They assumed a sharp, but continuous transition of permeability to connect different permeable media of constant permeabilities. The paper by van Duijn and de Neef [26] on the other hand, provided a semi-analytical solution for time-dependent countercurrent flow in 1D heterogeneous media with one discontinuity in permeability and capillary pressure. Niessner et al. [24] discuss the performance of some fully implicit vertex-centered finite volume schemes, when implementing the appropriate interface condition for capillary heterogeneous media. The recent paper by Hoteit and Firoozabadi [19] presents an MFE method for discretising the pressure equation together with a discontinuous Galerkin method for the saturation equation. They introduced a new fractional flow formulation for two-phase flow, which is suited for applying MFE in media with heterogeneous capillary pressure. Some numerical examples are presented, including a comparison with the 1D semi-analytical solution from [26], demonstrating good performance of the numerical scheme.

The simulation of two-phase flow in porous media with capillary pressure heterogeneity represents a challenge for the actual numerical discretization. This is particularly due to the fact that saturation discontinuities arise at the interface between the different homogeneous regions of the domain, as a result of the requirement of capillary pressure continuity. Moreover, since these are rather involved nonlinear problems, very few analytical results are known, making it more difficult to gain confidence in the results produced by the numerical schemes. Clearly, as discussed in [26], the capillary pressure may also actually become discontinuous at the interface in some situations. This depends on the form of the capillary pressure curve (the entry pressure) together with the actual type of two-phase flow in the problem. In the more usual situations where a wetting phase is displacing a non-wetting phase, this phenomenon will not occur. Moreover, since this particular situation does not introduce any new fundamental issues with respect to the numerical treatment of these problems, we only consider examples with capillary pressure continuity at the interface in this paper.

As noted in [19] MPFA methods have not yet been demonstrated to be of value for heterogeneous media with contrast in capillary pressure functions. This fact is a prime motivation for the present paper. We examine a standard scheme in 1D based on harmonic averaging of the absolute permeability as well as a more direct "naive" type of discretization and present detailed comparisons with the semi-analytical solutions from [26]. The scheme based on harmonic averaging of the absolute permeability, which can be considered as a "1D MPFA scheme", is found to converge and gives the best numerical results.

The "1D MPFA scheme" moreover, naturally provides a discrete approximation with a built-in pressure continuity. From the numerical results obtained in the 1D model problem, this property is considered to be important for the numerical treatment of these problems. Only recently, some multidimensional MPFA schemes with this property have been developed and tested for one-phase elliptic problems [13, 14, 16]. In this paper we extend the schemes from [13] and [16], which are developed for cell-centered quadrilateral and triangular grids, respectively, to two-phase flow problems, and also present some numerical examples. We use the recent fractional flow formulation

from [19], and moreover, solve the saturation equation by using the second-order central upwind scheme from [23].

The paper is organised as follows. Section 2 gives a description of the two-phase flow model, whereas Section 3 discusses two different implicit pressure explicit saturation (IMPES) formulations suitable for the numerical solution of this model. In Section 4 we study a 1D model problem using some different discretizations, and compare with semi-analytical solutions. Section 5 describes a recent discrete pressure continuous 2D MPFA scheme and its extension to two-phase flow. Furthermore, Section 6 briefly describes the central-upwind scheme used in the discretization of the saturation equation. Some numerical examples are presented in Section 7, that illustrate two-phase flow behavior with and without capillary pressure heterogeneity. Finally, conclusions follow in Section 8.

2. The two-phase flow model

In this section we present the governing equations for immiscible two-phase flow in a domain Ω of a porous medium. The mass balance equation for each of the fluid phases reads

$$\phi \frac{\partial(\rho_i s_i)}{\partial t} + \nabla \cdot (\rho_i \vec{u}_i) = \rho_i q_i, \qquad i = w, o, \tag{1}$$

where ϕ is the porosity of the medium, $i = w$ indicates the wetting phase (e.g. water) and $i = o$ indicates the nonwetting phase (e.g. oil). Moreover, ρ_i, s_i, $\vec{u}_i$ and q_i are, respectively, the density, saturation, velocity and external flow rate of the i-phase. The phase velocity is given by Darcy's law

$$\vec{u}_i = -\frac{k_{ri}}{\mu_i} \mathbf{K} \nabla (p_i - \rho_i g Z), \qquad i = w, o, \tag{2}$$

where $\mathbf{K}$ is the absolute permeability tensor of the porous medium, g is the gravitational constant and Z is the depth, i.e. the negative of the actual z-coordinate when the z-axis is in the vertical upward direction. p_i, μ_i and k_{ri} are, respectively the pressure, viscosity and relative permeability of the i-phase. Moreover, the capillary pressure is given by

$$P_c(\vec{x}, s_w) = p_o - p_w, \tag{3}$$

where $\vec{x}$ denotes the spatial coordinate vector, and the saturation constraint reads

$$s_w + s_o = 1. \tag{4}$$

It is useful to introduce the phase mobility functions

$$\lambda_i(\vec{x}, s_i) = \frac{k_{ri}}{\mu_i}, \qquad i = w, o,$$

the total mobility

$$\lambda(\vec{x}, s) = \lambda_w + \lambda_o,$$

and the total velocity

$$\vec{u} = \vec{u}_w + \vec{u}_o,$$

where $s = s_w$. Finally, the so called fractional flow functions f_i are defined as

$$f_i(\vec{x}, s) = \frac{\lambda_i}{\lambda}, \qquad i = w, o.$$

Usual boundary conditions for this model are the no-flow boundary conditions

$$\vec{u}_i \cdot \vec{n} = 0, \qquad i = w, o, \tag{5}$$

where $\vec{n}$ is the outer unit normal to the boundary $\delta\Omega$ of Ω. Alternatively, the flow rate(s) or oil pressure and water saturation may be prescribed at various parts of $\delta\Omega$.

3. IMPES formulations

We now reformulate the equations of Section 2 such that they become applicable for the IMPES formulation. Assuming the the fluids are incompressible, the equations (1) and (4) give rise to the following equation for the total velocity $\vec{u}$

$$\nabla \cdot \vec{u} = q_w + q_o \equiv q. \tag{6}$$

Using (6) together with equations (3) and (2) we obtain an elliptic equation for the pressure $p = p_o$, which reads

$$-\nabla \cdot (\lambda \mathbf{K} \nabla p) = -\nabla \cdot (\lambda_w \mathbf{K} \nabla P_c + (\lambda_w \rho_w + \lambda_o \rho_o) g \nabla Z) + q, \tag{7}$$

where the corresponding total velocity is given as

$$\vec{u} = -\mathbf{K}(\lambda \nabla p - \lambda_w \nabla P_c - (\lambda_w \rho_w + \lambda_o \rho_o) g \nabla Z). \tag{8}$$

Again using the assumption of incompressibility, an evolution equation for the saturation $s = s_w$ is obtained from equations (1) and (2) which reads

$$\phi \frac{\partial s}{\partial t} + \nabla \cdot (\mathbf{K} f_w(s) \lambda_o (\nabla P_c + (\rho_w - \rho_o) g \nabla Z) + f_w(s) \vec{u}) = q_w. \tag{9}$$

Observe that $P_c \neq 0$ gives us a convection-diffusion equation for the saturation s.

The IMPES solution strategy now goes as follows. For a given initial saturation $s(\vec{x}) = s_0(\vec{x})$, we solve the pressure equation (7), and then solve the saturation equation (9) based on the computed velocity field to update the saturation s. In the classical IMPES method the pressure and saturation fields are updated with the same frequency. However, since the saturation field usually changes more rapidly in time than the pressure field, it is natural to employ smaller time steps when solving the saturation equation.

In the improved IMPES method proposed by Chen et al. [10] the pressure equation is updated with a (possibly) variable time-step Δt_p, whereas the smaller variable inner time-steps Δt_s, used for the saturation equation, is determined by the relation

$$\Delta t_s = \frac{DS_{max}}{(\frac{\partial s}{\partial t})_{max}}, \tag{10}$$

where $(\frac{\partial s}{\partial t})_{max}$ denotes the maximum value of $\frac{\partial s}{\partial t}$ in the grid, and DS_{max} is the maximum variation of the saturation to allow. The latter quantity obviously needs to be specified from the outside. Note that the time-step determined by (10) obviously also must obey the CFL condition required by the underlying numerical scheme for the saturation equation.

By using this approach Chen et al. [10] obtained a considerable improvement of the classical IMPES method, and were i.a. able to solve a benchmark coning problem, previously unattainable for the classical IMPES formulation, 6.7 times faster than a comparative sequential solution method. We remark that Chen et al. [10] did not study problems including capillary pressure effects, which may seriously limit the usefulness of the IMPES formulation, due to the strict CFL conditions enforced by the usual explicit methods, e.g., Runge-Kutta methods, employed for the time-discretization of the saturation equation.

However, in this paper we are interested in a somewhat different fractional flow formulation, recently introduced by [19], which is also applicable for the IMPES solution strategy. In order to simplify the notation we first define the potentials

$$\Psi_i = p_i - \rho_i g Z, \qquad i = w, o, \tag{11}$$

and also the capillary pressure potential

$$\Psi_c = P_c - (\rho_o - \rho_w) g Z. \tag{12}$$

The idea in the new fractional flow formulation ([19]) is to introduce the velocities

$$\vec{u}_a = -\lambda \mathbf{K} \nabla \Psi_w, \tag{13}$$

and

$$\vec{u}_c = -\lambda_o \mathbf{K} \nabla \Psi_c. \tag{14}$$

It is now easily established that

$$\vec{u} = \vec{u}_a + \vec{u}_c,$$

and, moreover, that

$$\vec{u}_w = f_w(s)\vec{u}_a.$$

Equipped with this information, the pressure- and saturation equations in this new fractional flow formulation, may be expressed as

$$-\nabla \cdot (\lambda \mathbf{K} \nabla \Psi_w) = \nabla \cdot (\lambda_o \mathbf{K} \nabla \Psi_c) + q, \tag{15}$$

and

$$\phi \frac{\partial s}{\partial t} + \nabla \cdot (f_w(s)\vec{u}_a) = q_w. \tag{16}$$

where the potential Ψ_w and the water saturation s are the unknown variables, and the velocity $\vec{u}_a$ is given in equation (13). It should be noted that equation (16), in contrast to equation (9), is a pure convective equation. The capillary pressure effects are then exclusively connected to the pressure equation (15) in this formulation and does not at first sight influence the CFL condition in equation (16). However, the velocity $\vec{u}_a$ (produced from the pressure equation) is obviously a major contributor to the CFL requirement, and will thus nevertheless tighten the CFL requirement accordingly dependent on the degree of capillarity in the problem.

In this paper we employ the new fractional flow formulation, i.e. equations (15) and (16) above, for the simulation of two-phase flow with capillary pressure. Even though the old standard fractional flow formulation in principle could be used as well, the new formulation has some clear advantages. Obviously, the need for any nonlinear (Newtonian) iterations is eliminated, which is an advantage especially from the implementation point of view. Moreover, the new formulation also facilitates a much more straightforward implementation of the requirement of capillary pressure continuity at the interfaces between the different regions in the domain. Using the standard formulation, this task would have been more challenging, since it would also interact with the nonlinear iterative solution process.

4. Discretization in a 1D medium with a discontinuous capillary pressure function

Very few analytical solutions are known in heterogeneous porous media when capillarity is the driving force. In the paper [26], van Duijn and de Neef considered a 1D spontaneous imbibition model problem with a single discontinuity in permeability and capillary pressure. They searched for similarity solutions which amounts to transforming the original partial differential equation into an ordinary differential equations. More precisely, they obtained two ordinary differential equations (ODEs) that must fulfill two matching conditions at the discontinuity, and further produced a semi-analytical solution by solving the ODE problem numerically. For the purpose of testing the 1D discretizations discussed in this section, which serves as a motivation for the 2D MPFA finite-volume scheme presented in Section 5 and 6, we employ this semi-analytical approach.

The model problem we are interested in takes the form of a nonlinear diffusion equation given by

$$\frac{\partial s}{\partial t} + \frac{\partial}{\partial x}\Big(k(x) f_w(s) \lambda_o(s) \frac{\partial P_c(x,s)}{\partial x}\Big) = 0, \qquad x \in [-L, L]. \tag{17}$$

This equation is obtained from (9) by neglecting the gravity, setting total velocity and source term equal to zero, as well as assuming constant porosity ϕ to be 1 for the sake of simplicity only. Initial data $s_0(x) = s(x, t = 0)$ is given as

$$s_0(x) = \begin{cases} 1, & x < 0; \\ 0, & x > 0. \end{cases} \tag{18}$$

Furthermore, the permeability $k(x)$ is given by

$$k(x) = \begin{cases} k_l, & x < 0; \\ k_r, & x > 0. \end{cases} \tag{19}$$

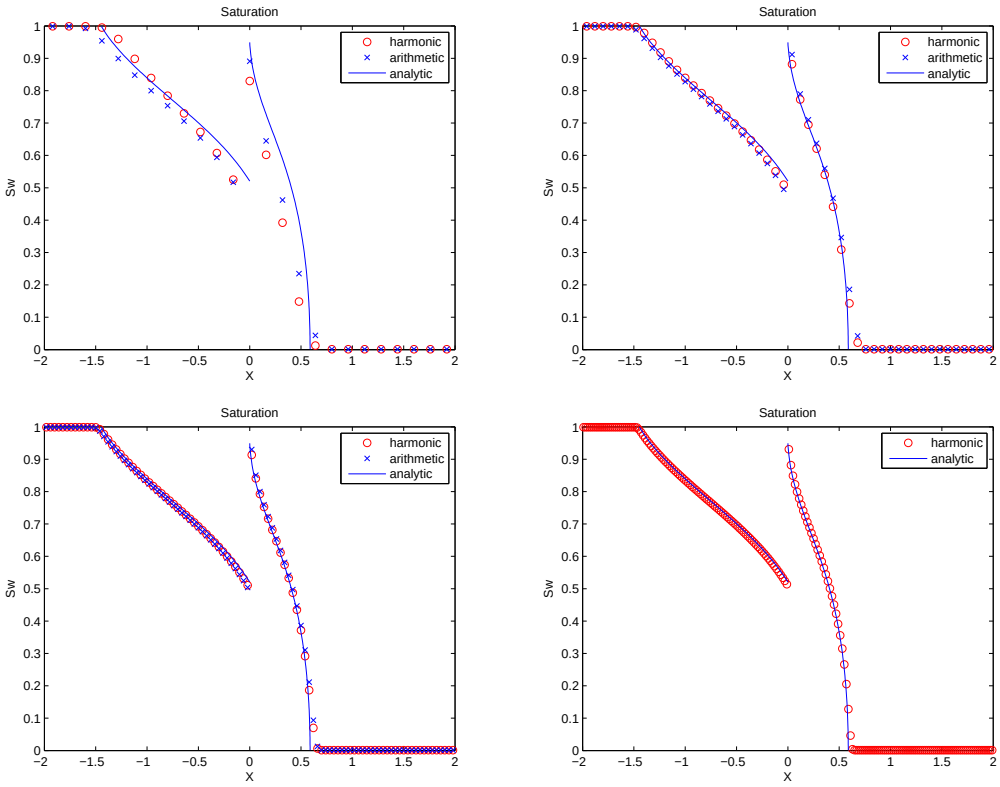

FIGURE 1. Computed solutions on different grids at time $T = 2$. Top left: 25 cells. Top right: 50 cells. Bottom left: 100 cells. Bottom right: 200 cells.

and $f_w(s)$ is the water fractional flow function $f_w(s) = \frac{\lambda_w(s)}{\lambda_w(s)+\lambda_o(s)}$ with the mobilities λ_w and λ_o defined as $\lambda_i = \frac{k_{ri}(s)}{\mu_i}$ for $i = w, o$. Moreover, the capillary pressure function P_c is given by

$$P_c(x, s) = \frac{1}{\sqrt{k(x)}} J(s), \tag{20}$$

where $J(s)$ is the Leverett function. Here we have implicitly set porosity ϕ and interfacial tension σ to be 1, for simplicity reasons only. In the following we also assume that the viscosity is characterized by $M = \frac{\mu_o}{\mu_w} = 1$. We consider the van Genuchten model, see [26] and references therein, where relative permeability and capillary pressure are given by

$$\begin{aligned} J(s) &= (s^{-1/m} - 1)^{1-m} \\ k_{rw}(s) &= s^{1/2}(1 - [1 - s^{1/m}]^m)^2 \\ k_{ro}(s) &= (1 - s)^{1/2}(1 - s^{1/m})^{2m}, \end{aligned} \tag{21}$$

where $0 < m < 1$ is a constant to be specified. In the numerical experiments carried out below we have used the following values

$$k_l = 4.2025, \qquad k_r = 0.5625, \qquad m = \frac{2}{3}. \tag{22}$$

Following the procedure outlined in [26] we solve for the similarity solution which we shall refer to as the analytical solution. This solution is used to evaluate the numerical approximation.

We consider a simple finite volume discretization for the numerical solution of the initial-value problem (17) and (18) with data as specified above. We discretize the spatial domain $\Omega = [-L, L]$ into N non-overlapping gridblocks Ω_i:

$$[-L, L] := \Omega = \cup_{i=1}^{N} \Omega_i, \qquad \Omega_i = [x_{i-1/2}, x_{i+1/2}], \qquad \Delta x_i = x_{i+1/2} - x_{i-1/2}.$$

	Harmonic		Arithmetic	
Δx	$\|E(s)\|_1$	q	$\|E(s)\|_1$	q
0.1600	0.1463	-	0.1351	-
0.0800	0.0332	-	0.0595	-
0.0400	0.0236	0.49	0.0390	0.61
0.0200	0.0178	0.41	0.0243	0.68
0.0100	0.0106	0.75	0.0133	0.87

TABLE 1. Estimated L^1-error, $\|E(s)\|_1 = \Delta x \sum_i |s_i - s_{\text{ref}}(x_i)|$, and convergence order, q, where s_{ref} is the reference solution obtained by solving the ODE system resulting from (17)–(19) and s_i refers to the numerical solution based on (23).

We assume, for simplicity, a regular grid with $\Delta x_i = \Delta x$. Similarly, we consider a constant time step size Δt. Given the water saturation $s^n \approx s(x, t^n)$ at time t^n, we must solve for the updated saturation s^{n+1} at time t^{n+1}. For that purpose we consider the discrete scheme

$$\frac{s_i^{n+1} - s_i^n}{\Delta t} + D_-\Big(k_{i+1/2}[f_w\lambda_o]^n_{i+1/2} D_+ P^n_{c,i}\Big) = 0, \qquad i = 1, \ldots, N, \tag{23}$$

where D_+ and D_- are the discrete differential operators applied on a sequence $\{a_i\}$ and defined by

$$D_+ a_i = \frac{a_{i+1} - a_i}{\Delta x}, \qquad D_- a_i = \frac{a_i - a_{i-1}}{\Delta x}.$$

Note that we have used a simple forward Euler discretization in time (explicit scheme). Consequently, we must also choose the time step according to the CFL condition

$$\frac{\Delta t}{\Delta x^2} \max(\sqrt{k_l}, \sqrt{k_r}) \max_i [f_w(s_i)\lambda_o(s_i)J'(s_i)] \leq \frac{1}{2}.$$

The average $[f_w\lambda_o]_{i+1/2}$ is obtained by taking an arithmetic average. For the average $k_{i+1/2}$ of the permeability function at the cell interface $i+1/2$ we check two different approaches: (i) arithmetic average k^A; (ii) harmonic average k^H.

$$k^A_{i+1/2} = \frac{k_i + k_{i+1}}{2}, \qquad k^H_{i+1/2} = \frac{2k_i k_{i+1}}{k_i + k_{i+1}}. \tag{24}$$

We have computed solutions at time $T = 2$ on three different grids corresponding to $N = 25$ cells, $N = 50$ cells, and $N = 75$ cells on a domain corresponding to $L = 2$. We refer to Fig. 1 for the results. The comparison between using k^A and k^H reveals that the harmonic averaging tends to give approximate solutions that lie closer to the analytical solution. Finally, we have also computed the solution on a finer grid of $N = 200$ cells by using the scheme with harmonic averaged permeability k^H demonstrating (virtually) convergence to the analytical solution. We refer also to Table 1 for estimates of the error measured in L^1-norm as the grid is refined. It seems that the rate of convergence is approaching 1. This relatively low rate of convergence is expected and must be understood in light of the severe discontinuity present in the solution.

It is well known (see e.g. [12]) that MPFA schemes in fact are generalizations of the scheme with harmonic averaging of the absolute permeability in higher spatial dimensions. Thus it is clear that the scheme which employs k^H automatically fulfills the requirement of continuity in capillary pressure at $x = 0$. However, for the sake of completeness of the paper, we present the arguments for this fact. For simplicity, we first consider the standard prototype pressure equation

$$\frac{d}{dx}(k\frac{dp}{dx}) = 0, \tag{25}$$

where p is the pressure. We are now interested in the discrete flux approximation produced by the one-dimensional MPFA scheme at $x_{i+1/2}$. The MPFA approach assumes piecewise linear pressure approximations i.e. such that

$$p = p_L(x) = p_i + a_L(x - x_i), \qquad \forall x \in [x_i, x_{i+1/2}], \tag{26}$$

and

$$p = p_R(x) = p_{i+1} + a_R(x_{i+1} - x), \qquad \forall x \in [x_{i+1/2}, x_{i+1}]. \tag{27}$$

Invoking the requirements of flux and pressure continuity at $x_{i+1/2}$ i.e.

$$k_i \frac{dp_L}{dx}(x_{i+1/2}) = k_{i+1} \frac{dp_R}{dx}(x_{i+1/2}), \qquad p_L(x_{i+1/2}) = p_R(x_{i+1/2}), \tag{28}$$

it is easily found that $a_L = \frac{2k_{i+1}}{k_{i+1}+k_i}(\frac{p_{i+1}-p_i}{\Delta x_i})$ and $a_R = \frac{2k_i}{k_{i+1}+k_i}(\frac{p_i-p_{i+1}}{\Delta x_i})$. The discrete flux at $x_{i+1/2}$ may thus be expressed as $\frac{2k_ik_{i+1}}{k_{i+1}+k_i}(\frac{p_{i+1}-p_i}{\Delta x_i})$, clearly showing the appearence of the harmonic average of the permeability $k^H_{i+1/2}$ as claimed above. Now looking at the term $\frac{\partial}{\partial x}\left(k(x)f_w(s)\lambda_o(s)\frac{\partial P_c(x,s)}{\partial x}\right)$ in (17). When this term is treated explicitly with respect to the saturation as in equation (23), it is clear that we can employ the same arguments with respect to the MPFA approximation as for the prototype pressure equation (25). Thus we can conclude that the capillary pressure is continuous at $x = 0$, when using the above scheme with k^H. Note that the fact that $[f_w\lambda_o]_{i+1/2}$ is approximated by an arithmetic average, obviously does not alter this conclusion.

Certainly, the more "naive" type of scheme which employs k^A, does *not* fulfill the requirement of continuity in capillary pressure at $x = 0$, and it is reasonable to expect that this fact explains the difference in the quality of the approximations revealed in Fig. 1. Even though the difference between these two approximations is relatively small, particularly for the fine grid with 100 cells, it is nevertheless important, since the only difference between these two numerical schemes in this particular example, is the flux approximation at $x = 0$. Realistic multidimensional examples on the other hand, requires reasonably coarse grids and can have numerous regions of capillary pressure heterogeneities throughout the domain, as well as significantly larger discontinuities than used in the present example, further emphasizing the importance of using numerical approximations fulfilling the requirement of capillary pressure continuity given by the continuous model.

However, standard multidimensional MPFA schemes are only pointwise pressure continuous at the discrete level. Only recently, some multidimensional MPFA schemes which are pressure continuous at the discrete level, have been developed and tested for one-phase elliptic problems [13, 14, 16]. These schemes are clearly favorable in cases with capillary pressure discontinuitues, and will thus be extended to two-phase flow in this paper.

5. A MPFA finite-volume discretization of the pressure equation

Two MPFA schemes fulfulling the property of being pressure continuous at the discrete level, henceforth denoted MPFA full pressure support (FPS) schemes, were recently presented in [13, 14] and [16] for cell-centered quardilateral and triangular grids, respectively. For completeness of presentation we present the MPFA FPS scheme for the one-phase pressure equation in case of cell-centered unstructured triangular grids. More details can be found in [16]. We then briefly comment on the extension of the scheme to two-phase flow.

5.1. **Notation.**

We now introduce appropriate notation for describing the family of unstructured cell-centred flux-continuous MPFA schemes employed in the paper.

5.1.1. *Grid Cell.* The grid (i.e. the collection of control-volumes or cells) is defined by the triangulation of the vertices (or corner points) j. Each grid cell is assigned a grid point (nodal point) $\mathbf{x_i}$, which here is equal to the cell centroid (see Figure 2(a)). In the cell-centered formulation presented here flow variables and rock properties are distributed to the grid cells and are therefore control-volume distributed (CVD). The value of the numerical solution in the cell is denoted by $\Phi_i = \phi_i(\mathbf{x_i})$. Two adjacent grid cells are termed neighbours if they share the same cell interface or cell edge. The permeability (conductivity) tensor K is assumed to be piecewise constant, with respect to cell values (see Figure 2(c)). The control-volume is denoted Ω_i for $i = 1, ..., N_E$, where N_E is the number of control-volumes (or cells) in the grid, and its corresponding boundary is $\delta\Omega_i$.

5.1.2. *Cluster.* In the cell centered formulation continuous flux and pressure constraints are imposed locally with respect to each *cluster* c_j of cells that are attached to a common grid vertex j. The *degree* of the *cluster* c_j is defined as the number of cell interfaces that meet at the vertex and is denoted by N_d^j. For each interior vertex the number of cells in the cluster is also equal to N_d^j. An example of a cell cluster with three cells and corresponding dual grid cell is shown in Figure 2(b).

5.1.3. *Dual-Cell.* For each cell cluster c_j, a *dual-cell* is defined as follows: For each cell edge attached to the vertex of the *cluster*, connect the edge mid-point e_k to the grid points (i.e. cell centres) of the two neighboring cells within the cluster that share the common edge (one cell centre if the edge is a boundary). It is not generally necessary to choose e_k as the mid-point, but in this paper other possibilities are not considered. The *dual-cell* will then be defined by the resulting polygon comprised of the contour segments connecting the N_d^j cell mid-points as indicated by the dashed lines in Figure 2(b).

5.1.4. *Sub-Cell.* Subcells result when the dual-cells overlay the primal triangular grid. Each triangle (control-volume) is then comprised of three quadrilateral *sub-cells*. Each sub-cell is defined by the anti-clockwise loop joining the parent triangle cell-centre, triangle right-edge mid-point, central cluster vertex, triangle left-edge mid-point and back to the triangle centre as illustrated in Figure 2(d). The volume of the *dual-cell* is seen to be comprised of N_d^j sub-cells, where each sub-cell of a parent triangle is attached to the same distinct vertex and thus cluster c_j.

5.1.5. *Sub-Interface.* The edge point e_k divides a cell interface into two segments, the term *sub-interface* will be used to distinguish each of the two segments from the total cell interface.

5.1.6. *Local Interface Pressures.* In the MPFA methods, the following two continuity conditions should be fulfilled for every *sub-interface*: flux continuity and pressure continuity. One of the main advantages of the this type of formulation is that it involves only a single degree of freedom per control-volume, in this case the primal grid cell pressure Φ_i, while maintaining continuity in pressure and normal flux across the control-volume faces. This is achieved by introducing local interface pressures that are expressed in terms of the global pressure field via local algebraic flux continuity conditions imposed across control-volume faces. In the MPFA FPS scheme full pressure continuity along each sub-interface in the grid is ensured by introducing an auxiliary interface pressure at the common grid vertex of the cluster as well as on each *sub-interface* (at point e_k) belonging to the *dual-cell*, thus yielding N_d^j+1 interface pressures per dual-cell. Referring to Figure 3, the interface pressures are denoted Φ_A, Φ_B, Φ_C and Φ_D, respectively. We remark that in the previous so called triangle pressure support formulations (TPS) (see e.g. [15]), the local interface pressures at the vertices were not employed, and the pressure is thus only point-wise continuous.

5.2. **Formulation in transform space.** We express the pressure equation in terms of a general curvilinear coordinate system with respect to dimensionless transform space coordinates (ξ, η) following [11]. Choosing Ω to represent an arbitrary control volume comprised of surfaces that are tangential to constant (ξ, η) respectively, the integral form of the pressure equation is written as

$$-\int_\Omega \tilde{\nabla} \cdot (\mathbf{T}\tilde{\nabla}\phi) d\tilde{\tau} = 0, \tag{29}$$

where $\tilde{\nabla} = (\frac{\partial}{\partial \xi}, \frac{\partial}{\partial \eta})$ and the general tensor $\mathbf{T}$ is defined via the Piola transform (see e.g. [7])

$$\mathbf{T} = \mid J \mid \mathbf{J}^{-1}\mathbf{K}\mathbf{J}^{-T}, \tag{30}$$

where $\mathbf{J}$ is the Jacobian of the curvilinear coordinate transformation and $\mid J \mid = x_\xi y_\eta - y_\xi x_\eta$ is the determinant of the Jacobian. $\mathbf{T}$ is thus a function of both the geometry- and cartesian permeability tensors, respectively, and its components are given by

$$\begin{aligned} T_{11} &= (K_{11} y_\eta^2 + K_{22} x_\eta^2 - 2K_{12} x_\eta y_\eta)/\mid J \mid \\ T_{22} &= (K_{11} y_\xi^2 + K_{yy} x_\xi^2 - 2K_{12} x_\xi y_\xi)/\mid J \mid \\ T_{12} &= (K_{12}(x_\xi y_\eta + x_\eta y_\xi) - (K_{11} y_\eta y_\xi + K_{22} x_\eta x_\xi))/\mid J \mid \end{aligned} \tag{31}$$

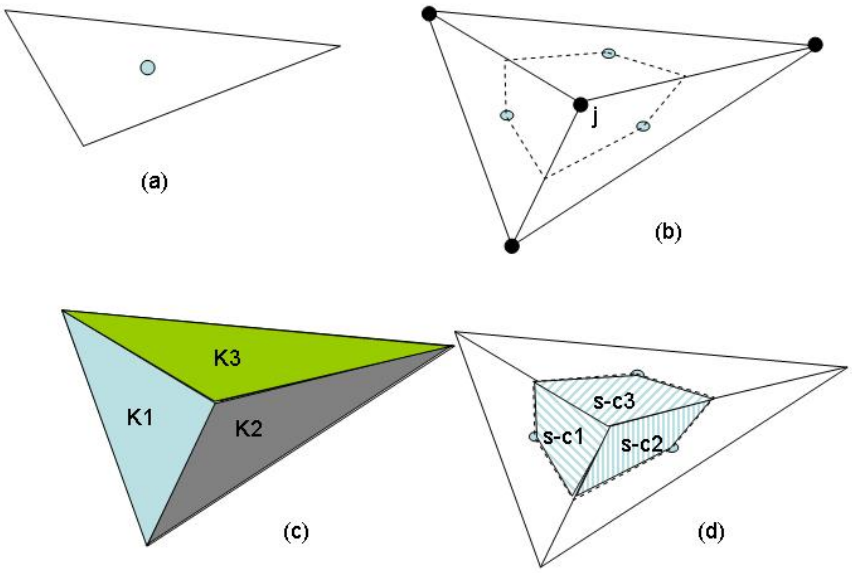

FIGURE 2. (a) Triangular control-volume with cell-centered nodal point. (b) Dual-cell (dashed lines) defined for cell *cluster* containing 3 *sub-cells* at vertex j. (c) Piecewise constant permeability over triangular control volumes. (d) The *sub-cells* in a dual-cell. Shade indicates sub-cell.

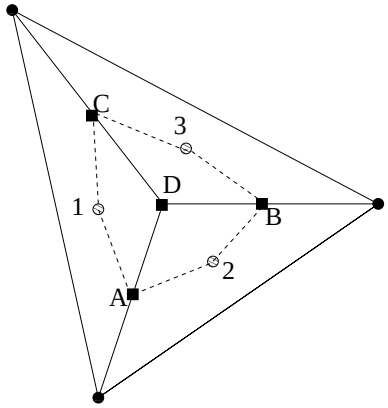

FIGURE 3. The interface pressures indicated by squares at positions A, B, C and D in the cell *cluster*.

Equation (29) can also be written as

$$-\int_{\Omega}(\frac{\partial \mathrm{F}_1}{\partial \xi_1}+\frac{\partial \mathrm{F}_2}{\partial \xi_2})d\tilde{\tau}=0, \tag{32}$$

where the local flux is given by

$$\mathrm{F}_i=-\int\sum_{j=1}^{2}T_{i,j}\phi_{\xi_j}d\Gamma_i, \tag{33}$$

where $T_{i,j}$ are defined in Eq. (31), ξ_j used as a subscript denotes partial differentiation in the ξ_j-direction, $\xi_1=\xi$ and $\xi_2=\eta$.

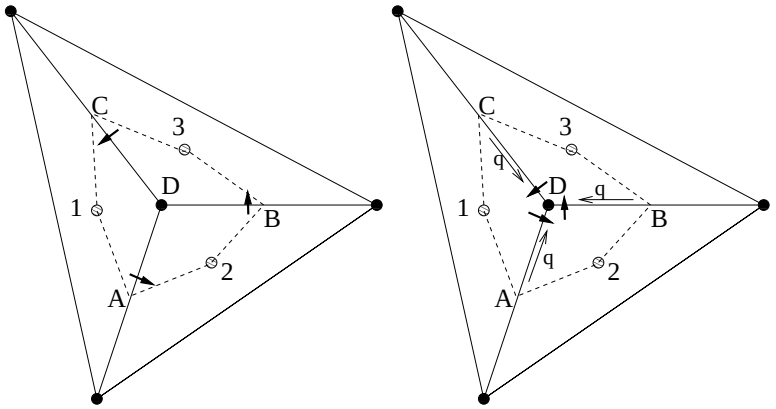

FIGURE 4. Left: The direction of the fluxes indicated by arrows at the sub-interfaces. Right: Quadrature parametrization indicating point-wise flux evaluation for a given value of the parameter q.

We now introduce a local *right-handed* (ξ, η)-coordinate system in each sub-cell, and the problem is then to solve the following integrated pressure equation for a triangular grid

$$-\sum_{s=1}^{3}(\int_{\delta\tilde{\Omega}_i^s}(T^s\tilde{\nabla}\phi)\cdot\vec{n}_t^s d\Gamma) = 0, \tag{34}$$

where the superscript s is connected to a given (quadrilateral) sub-cell within the triangle (see Figure 2(d)), $\vec{n}_t^s$ is the transform space sub-cell normal vector and $\delta\tilde{\Omega}_i^s$ denotes the outer boundary of the sub-cell in transform space.

In general the sub-cell tensor can be defined via the isoparametric mapping

$$\vec{r} = (1-\xi)(1-\eta)\vec{r}_1 + \xi(1-\eta)\vec{r}_2 + \xi\eta\vec{r}_3 + (1-\xi)\eta\vec{r}_4 \tag{35}$$

where $\vec{r} = (x, y)$, $\vec{r}_i, i = 1, ...4$ are the subcell corner position vectors and $0 \leq \xi, \eta \leq 1$, with $\vec{r}_1$ and $\vec{r}_3$ corresponding to the cell-centre and dual-cell centre respectively and $\vec{r}_2$ and $\vec{r}_4$ correspond to the mid-points of the triangle edges connected to the dual-cell centre. As a result each quadrilateral subcell is transformed into a unit quadrant in transform space. The tensor is then approximated in a local coordinate system aligned with the two faces of the dual-cell connected to the given sub-cell.

5.3. **The MPFA FPS approximation.** Assuming a bi-linear approximation within each sub-cell (Figure 3), the pressures in the three sub-cells may be written in the local (ξ, η)-coordinate-system as

$$\phi_1 = \Phi_1 + (\Phi_A - \Phi_1)\xi + (\Phi_C - \Phi_1)\eta + (\Phi_D + \Phi_1 - \Phi_A - \Phi_C)\xi\eta, \tag{36}$$

$$\phi_2 = \Phi_2 + (\Phi_B - \Phi_2)\xi + (\Phi_A - \Phi_2)\eta + (\Phi_D + \Phi_2 - \Phi_B - \Phi_A)\xi\eta, \tag{37}$$

and

$$\phi_3 = \Phi_3 + (\Phi_C - \Phi_3)\xi + (\Phi_B - \Phi_3)\eta + (\Phi_D + \Phi_3 - \Phi_C - \Phi_B)\xi\eta. \tag{38}$$

Physical space flux continuity conditions are defined with respect to each cell cluster. We define the fluxes in a counter-clock wise manner with respect to the *sub-interfaces* of each cluster. Now let D denote the cluster vertex in the illustrative cluster shown in Figure 4(left). We let F_A be the flux out of cell 1 through the *sub-interface* at AD, F_B be the flux out of cell 2 through the *sub-interface* at BD and F_C be the flux out of cell 3 through the *sub interface* at CD (see Figure 4(left)).

Introducing a quadrature parametrization q such that $0 \leq q \leq 1$ (see Figure 4(right)), the point-wise flux continuity is accommodated along each of the lines AD, BD and CD, respectively.

Utilizing equation (33), the three flux continuity equations then read

$$\begin{aligned} F_{AD} &= -(T_{11}|^1_{AD(q)}(\Phi_A-\Phi_1)+(\eta T_{11})|^1_{AD(q)}(\Phi_D+\Phi_1-\Phi_A-\Phi_C) \\ &+ T_{12}|^1_{AD(q)}(\Phi_C-\Phi_1)+T_{12}|^1_{AD(q)}(\Phi_D+\Phi_1-\Phi_A-\Phi_C)) \\ &= T_{12}|^2_{AD(q)}(\Phi_B-\Phi_2)+T_{12}|^2_{AD(q)}(\Phi_D+\Phi_2-\Phi_B-\Phi_A) \\ &+ T_{22}|^2_{AD(q)}(\Phi_A-\Phi_2)+(\xi T_{22})|^2_{AD(q)}(\Phi_D+\Phi_2-\Phi_B-\Phi_A), \end{aligned} \tag{39}$$

$$\begin{aligned} F_{BD} &= -(T_{11}|^2_{BD(q)}(\Phi_B-\Phi_2)+(\eta T_{11})^2_{BD(q)}(\Phi_D+\Phi_2-\Phi_B-\Phi_A) \\ &+ T_{12}|^2_{BD(q)}(\Phi_A-\Phi_2)+T_{12}|^2_{BD(q)}(\Phi_D+\Phi_2-\Phi_B-\Phi_A)) \\ &= T_{12}|^3_{BD(q)}(\Phi_C-\Phi_3)+T_{12}|^3_{BD(q)}(\Phi_D+\Phi_3-\Phi_C-\Phi_B) \\ &+ T_{22}|^3_{BD(q)}(\Phi_B-\Phi_3)+(\xi T_{22})^3_{BD(q)}(\Phi_D+\Phi_3-\Phi_C-\Phi_B), \end{aligned} \tag{40}$$

and

$$\begin{aligned} F_{CD} &= -(T_{11}|^3_{CD(q)}(\Phi_C-\Phi_3)+(\eta T_{11})^3_{CD(q)}(\Phi_D+\Phi_3-\Phi_C-\Phi_B) \\ &+ T_{12}|^3_{CD(q)}(\Phi_B-\Phi_3)+T_{12}|^3_{CD(q)}(\Phi_D+\Phi_3-\Phi_C-\Phi_B)) \\ &= T_{12}|^1_{CD(q)}(\Phi_A-\Phi_1)+T_{12}|^1_{CD(q)}(\Phi_D+\Phi_1-\Phi_A-\Phi_C) \\ &+ T_{22}|^1_{CD(q)}(\Phi_C-\Phi_1)+(\xi T_{22})^1_{CD(q)}(\Phi_D+\Phi_1-\Phi_A-\Phi_C). \end{aligned} \tag{41}$$

Note that the notation $AD(q)$ etc. serves to indicate the dependence of the flux continuity point on the quadrature parametrization. Note that $AD(0)=A$ and $AD(1)=D$, while $0<q<1$ extracts points $\vec{P}$ along the line AD such that $\vec{P}=\vec{A}+q(\vec{D}-\vec{A})$ (and of course analogously along the lines BD and CD).

However, in order to close the above equation system (39), (40) and (41) an additional equation is needed. For that purpose we utilize the integral form of the partial differential equation over an auxillary dual-cell (see Figure 5(left)) i.e.

$$-\oint_{\delta\tilde{\Omega}^d_{jAUX}}(\mathbf{T}\tilde{\nabla}\phi)\cdot\vec{n}_t d\Gamma=0, \tag{42}$$

where $\tilde{\Omega}^d_{jAUX}$ denotes the (transform space) auxillary dual-cell connected to a vertex with index j. The actual size of the auxillary dual cell control-volume is a further degree of freedom to be chosen within the scheme, and is parameterized by the variable c where $0\leq c\leq 1$. Note that for $c=0$ we obtain the usual dual-cell, while the auxillary control-volume tends to zero as $c\to 1$. Yet another free parameter is needed to specify this scheme. We let p be the quadrature parametrization needed for the point-wise flux evaluation needed at the sub-interfaces in the auxillary dual-cell in equation (42). p should be chosen such that $c\leq p<1$. Discretisizing equation (42) following the above sub-cell approach, we then obtain a dual-cell equation which reads

$$\begin{aligned} & T_{11}|^1_{C1(c,p)}(\Phi_A-\Phi_1)+(\eta T_{11})^1_{C1(c,p)}(\Phi_D+\Phi_1-\Phi_A-\Phi_C) \\ + \; & T_{12}|^1_{C1(c,p)}(\Phi_C-\Phi_1)+(\xi T_{12})^1_{C1(c,p)}(\Phi_D+\Phi_1-\Phi_A-\Phi_C) \\ + \; & T_{12}|^1_{1A(c,p)}(\Phi_A-\Phi_1)+(\eta T_{12})^1_{1A(c,p)}(\Phi_D+\Phi_1-\Phi_A-\Phi_C) \\ + \; & T_{22}|^1_{1A(c,p)}(\Phi_C-\Phi_1)+(\xi T_{22})^1_{1A(c,p)}(\Phi_D+\Phi_1-\Phi_A-\Phi_C) \\ + \; & T_{11}|^2_{A2(c,p)}(\Phi_B-\Phi_2)+(\eta T_{11})^2_{A2(c,p)}(\Phi_D+\Phi_2-\Phi_B-\Phi_A) \\ + \; & T_{12}|^2_{A2(c,p)}(\Phi_A-\Phi_2)+(\xi T_{12})^2_{A2(c,p)}(\Phi_D+\Phi_2-\Phi_B-\Phi_A) \\ + \; & T_{12}|^2_{2B(c,p)}(\Phi_B-\Phi_2)+(\eta T_{12})^2_{2B(c,p)}(\Phi_D+\Phi_2-\Phi_B-\Phi_A) \\ + \; & T_{22}|^2_{2B(c,p)}(\Phi_A-\Phi_2)+(\xi T_{22})^2_{2B(c,p)}(\Phi_D+\Phi_2-\Phi_B-\Phi_A) \\ + \; & T_{11}|^3_{B3(c,p)}(\Phi_C-\Phi_3)+(\eta T_{11})^3_{B3(c,p)}(\Phi_D+\Phi_3-\Phi_C-\Phi_B) \\ + \; & T_{12}|^3_{B3(c,p)}(\Phi_B-\Phi_3)+(\xi T_{12})^3_{B3(c,p)}(\Phi_D+\Phi_3-\Phi_C-\Phi_B) \\ + \; & T_{12}|^3_{3C(c,p)}(\Phi_C-\Phi_3)+(\eta T_{12})^3_{3C(c,p)}(\Phi_D+\Phi_3-\Phi_C-\Phi_B) \\ + \; & T_{22}|^3_{3C(c,p)}(\Phi_B-\Phi_3)+(\xi T_{22})^3_{3C(c,p)}(\Phi_D+\Phi_3-\Phi_C-\Phi_B) \\ = \; & 0, \end{aligned} \tag{43}$$

where the notation $C1(c,p)$, $1A(c,p)$ etc serves to indicate the dependence of the parameters c and p on the position of the discrete flux evaluation on the half edges in the auxillary dual cell, which are parallel with the lines $C1$, $1A$ (see Figure 5(right)) etc. in transform space. Note that

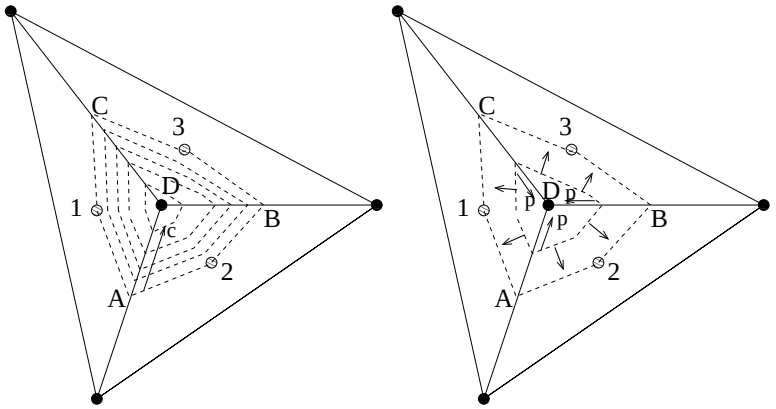

FIGURE 5. Left: Example range of auxillary control volumes (dashed) centered around the vertex D and depending on the parameter c. Right: Fluxes out of auxillary dual cell and quadrature parametrization indicating point-wise flux evaluation for a given value of the parameter p at the sub-interfaces in the auxillary dual-cell.

$C1(0,0) = C$, $1A(0,0) = 1$ (where 1 in this last equation obviously means the triangle centroid of cell 1 in Figure 5(right)).

The equations (39), (40), (41) and (43) now define a linear system of equations in terms of dual-interface pressures and the primal cell-centered pressures for all cells connected to the cluster vertex. This system may generally be written as follows

$$M_f \mathbf{\Phi_f} = M_c \mathbf{\Phi_c}, \tag{44}$$

where M_f and M_c are matrices. In this particular case of a three cell cluster $\mathbf{\Phi_f} = (\Phi_A, \Phi_B, \Phi_C, \Phi_D)^T$ and $\mathbf{\Phi_c} = (\Phi_1, \Phi_2, \Phi_3)^T$. Obviously this may be done analogously for an arbitrary cell cluster. Thus the interface pressures can be expressed in terms of the primal cell-centered pressures via equation (44), which is performed in a preprocessing step thus eliminating them from the discrete system.

5.4. **Flux and finite volume approximation.** Utilizing the above local algebraic flux contiuity conditions, the discrete flux F across a cell sub-interface in the grid may be written as a linear combination of grid cell centre values Φ_i in the dual grid:

$$F = -\sum_{i \in N_F^j} t_i \Phi_i, \tag{45}$$

where N_F^j is the index set of grid points involved in the flux approximation and N_F^j contains a maximum of N_d^j cells. The coefficients t_i resemble conductances and are called the *transmissibilities* associated with the flux interface. Since the flux must be zero when Φ_i is constant for all $i \in N_F^j$, all consistent discretizations must satisfy the condition $\sum_{i \in N_F^j} t_i = 0$. The net flux across each cell-interface (triangle-edge) is comprised of two sub-interface fluxes, calculated by assembling contributions from the two dual grid cells corresponding to the two triangle-edge vertices.

Finally the discrete divergence over the primal triangle cells is then comprised of assembled fluxes that are algebraically linear functions of the primal cell-centered pressures. This defines the so called MPFA FPS scheme recently presented in [16], for elliptic problems.

5.5. **Extensions to account for two-phase flow.** Untill now we have presented the discretization methodology for the one-phase flow pressure equation. However, the extension needed to

treat the present two-phase flow flux term i.e.

$$-\oint_{\delta\Omega_i}(\lambda(s)\mathbf{K}\nabla\Psi_w)\cdot\vec{n}dS$$

is indeed very limited. Let λ_v represent the total mobility at the vertex v in the grid, which can be found by the interpolation procedure i.e. equation (56), described in Section 6 below. Since the mobility λ is a scalar quantity, a two-phase flow sub-interface flux F_{tf} can then be written as

$$F_{tf} = \lambda_v F, \tag{46}$$

where F is the flux given in equation (45), which obviously is supposed to belong to the cluster with vertex v. Alternatively, from an implemenation point of view, it is sufficient to multiply the transmissibilities in equation (45) with λ_v.

5.6. **Approximating the capillary pressure flux.** The capillary pressure flux, which is a right hand side contribution in the integrated form of the pressure equation, reads

$$\oint_{\delta\Omega_i}(\lambda_o\mathbf{K}\nabla\Psi_c)\cdot\vec{n}dS.$$

It can be approximated by the MPFA FPS scheme as follows. Assume that a saturation field is given in the control-volume cell centers such that we know the cell centered capillary pressures, and consider the scheme described in Section 5.3 (except that the transmissibilites must be multiplied with λ_{ov}, where v again is an index identifying the vertex). Due to the construction of the MPFA FPS algorithm the capillary pressure field will be continuous (which is physically correct) and the capillary pressure flux over a given sub-interface F_{tcp} simply reads

$$F_{tcp} = \lambda_{ov} F, \tag{47}$$

where the flux F (given in equation (45)) now can be computed explicitly from known cell-centered capillary pressure potentials Ψ_c.

Remark 1. *As noted in the introdution, there are in fact cases i.a. depending on the entry pressure and the type of flow, where the capillary pressure may be discontinuous at interfaces between different rock types (even if continuity in capillary pressure is the usual situation). See* [26] *for a more detailed discussion. In such cases the MPFA FPS scheme will have to be modified, by introducing a double set of auxillary pressures in the formulation. Additional equations will then be needed to close the local equation system. Such equations may be found from knowledge of the saturation values in some parts of the domain. However, we emphasize that this situation can not occur in the cases considered in this paper where water is displacing oil, and, moreover, do not introduce any new fundamental issues with respect to the numerical treatment of these problems,*

5.7. **Computing the velocity $\vec{v}_a$.** When Ψ_w is found by solving the pressure equation (15) using the MPFA FPS scheme, the velocity $\vec{v}_a = -\lambda\mathbf{K}\nabla\Psi_w$, or more precisely the flux of $\vec{v}_a$ over a given interface in the grid, must be computed in order to be used as input in the saturation equation (16). This can be done by computing each of the sub-interface fluxes, which in this case can be computed explicitly from equation (46).

6. Discretization of the saturation equation

The relatively recent so called central-upwind schemes for hyperbolic conservation laws were introduced in [22]. These schemes extend the central schemes developed by Kurganov and Tadmor in [21], and in fact coincide for a scalar PDE such as the saturation equation. The central-upwind schemes belong to the class of Godunov-type central schemes, and their construction is based on the exact evolution of picewise polynomial reconstructions of the approximate solution, achieved by integrating over Riemann fans. Their resolution is comparable to the upwind schemes, but in contrast to the latter, they do not employ Riemann solvers and characterisitic decomposition, which makes them both simple and efficient for a variety of multidimensional PDE systems.

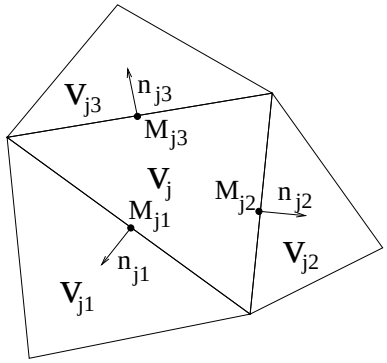

FIGURE 6. Notation in a triangular grid.

For the case of unstructured triangular grids a (second-order) central-upwind scheme was recently presented in [23]. In this paper we employ the scheme from [23] for the spatial semi-discretization of the saturation equation. In the following we present some details pertaining to this discretization.

Consider as an example the scalar conservation law

$$\frac{\partial s}{\partial t} + \frac{\partial f(s)}{\partial x} + \frac{\partial g(s)}{\partial y} = 0. \tag{48}$$

In order to introduce some necessary notation, let us denote the control volumes in the triangulation by V_j, with corresponding areas ΔV_j. For a given index j, the neighbouring control volumes of V_j are termed V_{jk}, $k = 1, 2, 3$. Moreover, the joint edge between V_j and V_{jk} is denoted by E_{jk} and is assumed to be of length h_{jk}. Finally, the outward unit normal to V_j on the kth edge is n_{jk}, and the midpoint of E_{jk} is M_{jk} (see Figure 6).

Now let

$$\bar{s}_j^n \approx \frac{1}{\Delta V_j} \int_{v_j} s(\vec{x}, t^n) dV \tag{49}$$

be the cell average on all the cells $\{V_j\}$, which are assumed to be known at the time t^n, and let

$$\tilde{s}^n(x, y) = \sum_j s_j^n(x, y) \chi_j(x, y) \tag{50}$$

be a reconstructed piecewise polynomial, where $\chi_j(x, y)$ is the characteristic function of the control volume V_j, $s_j^n(x, y)$ is a two-dimensional polynomial yet to be determined and, finally, $s_{jk}^n(x, y)$ denotes the corresponding polynomial that is reconstructed in the control volume V_{jk}.

Discontinuities in the interpolant s_j along the edges of V_j (where we for simplicity omit time dependence n and spatial dependence (x, y)) propagate with a maximal inward velocity and a maximal outward velocity a_{jk}^{in} and a_{jk}^{out}, respectively. For convex fluxes in the scalar case these fluxes can be estimated as

$$a_{jk}^{in}(M_{jk}) = -\min\{\nabla F(s_j(M_{jk})) \cdot n_{jk}, \nabla F(s_{jk}(M_{jk})) \cdot n_{jk}, 0\},$$
$$a_{jk}^{out}(M_{jk}) = \max\{\nabla F(s_j(M_{jk})) \cdot n_{jk}, \nabla F(s_{jk}(M_{jk})) \cdot n_{jk}, 0\},$$

where $F = (f, g)$.

Now the algorithmic development of the central-upwind scheme goes as follows. The above local speeds of propagation are used to determine evolution points that are away from the propagating discontinuities. An exact evolution of the reconstruction at these evolution points is followed by an intermediate piecewise polynomial reconstruction and finally projected back onto the original control volumes, providing the cell averages at the next time step $\bar{s}_j^{n+1}$.

A semi-discrete scheme is then obtained at the limit

$$\frac{d}{dt}\bar{s}^n = \lim_{\Delta t \to 0} \frac{\bar{s}^{n+1} - \bar{s}^n}{\Delta t}. \tag{51}$$

Fortunately most of the terms on the right-hand side of (51) vanish in the limit as $\Delta t \to 0$, leaving only the integrals of the flux functions over the edges of the cells, which must be determined by an appropriate quadrature. We follow [23] and use a simple midpoint quadrature, which leads to the following semi-discrete scheme

$$\frac{d}{dt}\bar{s}^n = -\frac{1}{\Delta V_j}\sum_{k=1}^{3}\frac{h_{jk}}{a_{jk}^{in}+a_{jk}^{out}}[(a_{jk}^{in}F_{jk}^{out}+a_{jk}^{out}F_{jk}^{in})\cdot n_{jk} - a_{jk}^{in}a_{jk}^{out}(s_{jk}^{out}-s_{jk}^{in})], \tag{52}$$

where we have employed the notation $s_{jk}^{out} = s_{jk}(M_{jk})$, $s_{jk}^{in} = s_j(M_{jk})$, $F_{jk}^{in} = F(s_{jk}^{in})$ and $F_{jk}^{out} = F(s_{jk}^{out})$. We refer to [23] for more details about this scheme, which can be applied to systems of conservation laws in an analogous manner.

The particular second-order reconstruction used in this paper is taken from [8]. The first step is to compute a least-squares estimate of the gradient of a scalar field f on the triangle V_j, which is denoted by $\tilde{\nabla}_j f$. $\tilde{\nabla}_j f$ is computed by following the algorithm reported in [3]. The gradient $\mathcal{D}_j f$ are then limited component by component as

$$\mathcal{D}_j f = \mathcal{MM}(\tilde{\nabla}_j f, \tilde{\nabla}_{j1} f, \tilde{\nabla}_{j2} f, \tilde{\nabla}_{j3} f), \tag{53}$$

where $\tilde{\nabla}_{jk} f$ is the least-squares gradient estimate on V_{jk} and $\mathcal{MM}$ is the common multivariable MinMod limiter function defined by

$$\text{MinMod}(x_1, x_2, \ldots) := \begin{cases} \min_j\{x_j\} & \text{if } x_j > 0 \ \forall j, \\ \max_j\{x_j\} & \text{if } x_j < 0 \ \forall j, \\ 0 & \text{otherwise.} \end{cases} \tag{54}$$

Furthermore, the gradients $\mathcal{D}_j f$ is used to construct a piecewise linear reconstruction for the point values of each triangle edge E_{jk} as follows

$$u_j(\vec{x}) = \bar{u}_j + \mathcal{MM}(\mathcal{D}_j u \cdot (\vec{x} - \vec{x}_j), \mathcal{D}_{jk} u \cdot (\vec{x} - \vec{x}_j)), \tag{55}$$

where $\mathcal{D}_{jk} u$ is the limited gradient estimate on V_{jk}, $\vec{x}_j$ is the center of V_j and $\vec{x} \in E_{jk}$. As noted in [8], this double use of the MinMod limiter minimizes spurious oscillations while preserving the second-order accuracy of the reconstruction.

6.1. **Interpolation of the mobility.** In Sections 5.5 and 5.6 an interpolation of the mobility (λ or λ_0, respectively) from the cell-centered values is needed at the vertices in the grid. This is done by the following formula

$$\lambda_v = \frac{\sum_{i:V_i \in \mathcal{V}_{vi}}(\lambda_i \Delta V_i)}{\sum_{i:V_i \in \mathcal{V}_{vi}}(\Delta V_i)}, \tag{56}$$

where λ_v is the mobility at the vertex v and $\mathcal{V}_{vi}$ denotes the set of triangles neighbouring this same vertex.

7. Computational examples

In the following we present two examples demonstrating effects of capillary pressure heterogeneity in two-phase flow using a structured cartesian grid and an unstructured triangulation, respectively. Here we consider a capillary pressure function of the form

$$P_c(s) = -\frac{\phi}{\sqrt{k}} ln(s), \tag{57}$$

where k is the absolute permeability and the capillary pressure curves are truncated to a finite large value at $s = 0$, in order to avoid infinity values at that point. Further we use quadratic Corey-type relative permeability curves i.e.

$$k_{rw}(s) = s^2, \qquad k_{ro}(s) = (1-s)^2. \tag{58}$$

Moreover for simplicity reasons only, we put $\phi = 1$, $\mu_w = \mu_o = 1$, $L^* = 1$ and $k^* = 1$, where L^* and k^*, respectively, are chosen as the characteristic length and absolute permeability in the problems below. We would like to emphasize that these examples are totally synthetic, their purpose being only to illustrate some flow phenomena connected to the presence of capillary

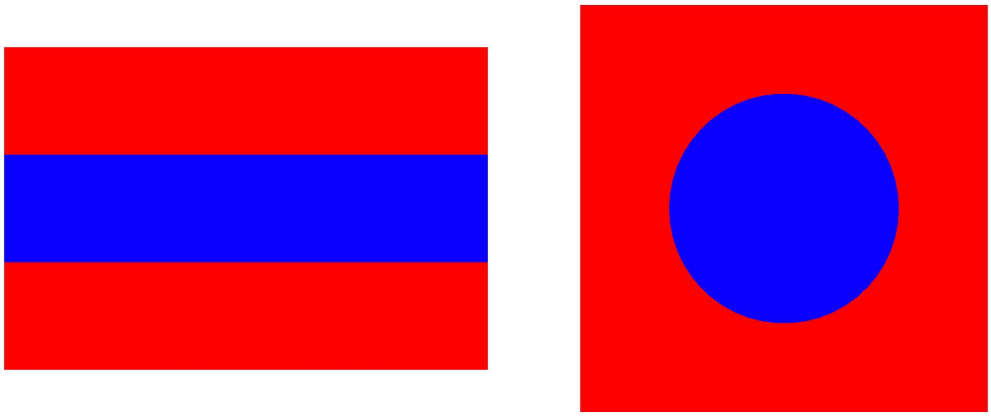

FIGURE 7. Left: The domain in example 1. The middle layer is least permeable. Right: The domain in example 2. The circular inclusion is least permeable.

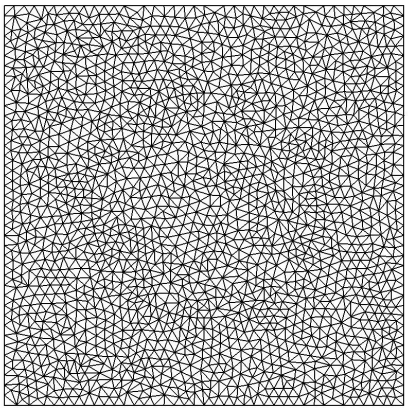

FIGURE 8. The unstructured triangulation used in example 2.

pressure heterogeneity in two spatial dimensions. Computations using real reservoirs are outside the scope of this paper.

The computations on triangular grids in Example 2 below are performed by using the MPFA FPS scheme presented above, while the computations on the structured grid in Example 1 employs the corresponding scheme for quadrilaterals [13]. The application of these recent MPFA FPS schemes in the following two-phase flow computations are particularly important for two reasons. Firstly, it was found in a recent study [17], that the previous classes of MPFA schemes, which are only pointwise continuous in pressure and flux, do not exhibit convergent behavior for time-dependent diffusion problems on triangular grids. Secondly, as thoroughly discussed in Section 4, a full pressure continuity at the discrete level is important in order to mimic the important requirement of capillary pressure continuity at the continuous level in problems with capillary pressure heterogeneity.

7.1. **Example 1.** We consider displacement of oil by water in the $0.5 \times \frac{1}{3}$ layered rectangular domain, initially filled with oil, which is shown in Figure 7 (left). The isotropic permeability is equal to 0.01 in the middle layer and 1 otherwise. Water is injected uniformly through the left vertical boundary, and the boundary conditions are as follows. The two horizontal boundaries are closed, and the oil pressure difference between the right and left vertical boundaries is put to 1.

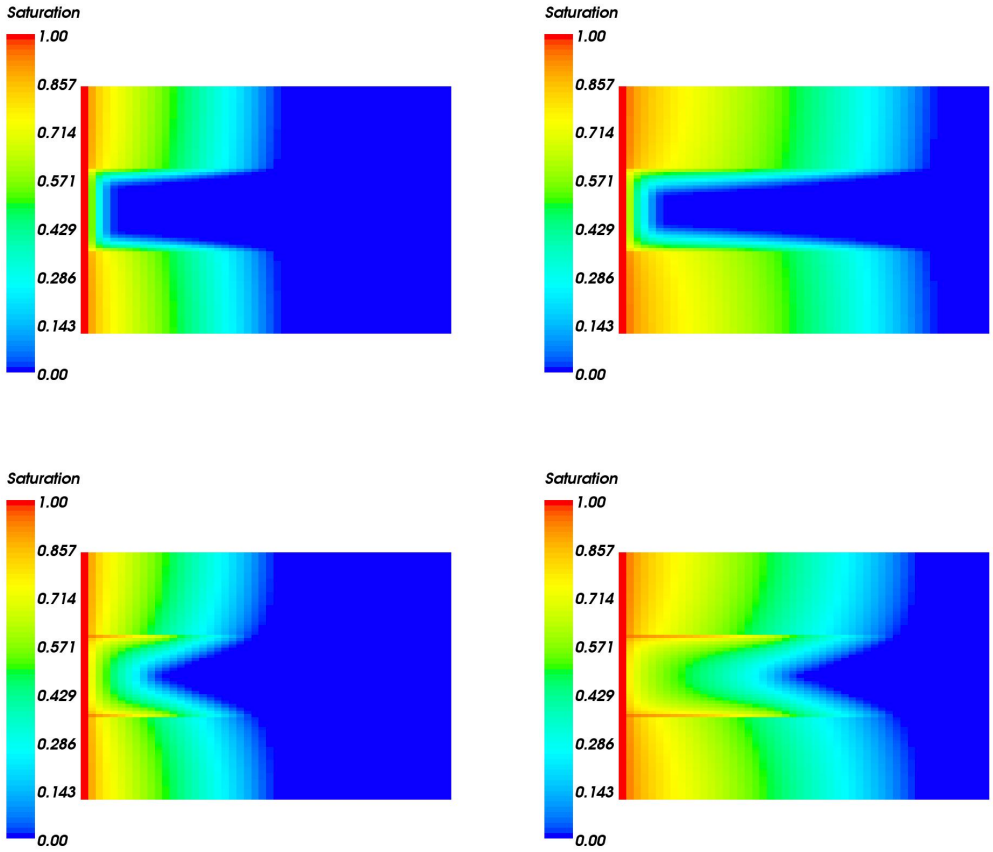

FIGURE 9. Example of solution fields from example 1. Top row: Homogeneous capillary pressure. Bottom row: Heterogeneous capillary pressure. Left column: $t = 0.03$. Right column: $t = 0.07$.

Moreover, we impose a saturation equal to 1 at the left vertical boundary, whereas the saturation is put to 0 at the right vertical boundary.

Numerical computations (with a 50×75 structured rectangular grid) are performed using both a capillary homogeneous (k is put to 1 in equation (57)) and capillary heterogeneous domain. Results are presented in Figure 9 for two different simulation times. The flow behavior with homogeneous capillary pressure is as expected essentially governed by the permeability field such that the displacement process is very much delayed in the middle low permeability layer, and, moreover exhibits a smooth behavior typical of standard diffusion problems.

The simulation results in the case of capillary pressure heterogeneity on the other hand, demonstrates a substantially more complex flow behavior. In particular, we observe saturation discontinuites that have arosen at the two boundaries of the middle low permeability layer. Furthermore, it is clearly seen that water has penetrated the low permeable domain to a much wider extent than in the case with homogeneous capillary pressure.

7.2. **Example 2.** The 2×2 quadratic domain with a circular inclusion as well as the unstructured grid with 3738 triangles is shown in Figure 7 (right) and Figure 8, respectively. The isotropic permeability is equal to 0.01 in the circular inclusion and 1 otherwise. The four boundaries are closed in this example. Water is injected at the lower left corner in the domain (source strength

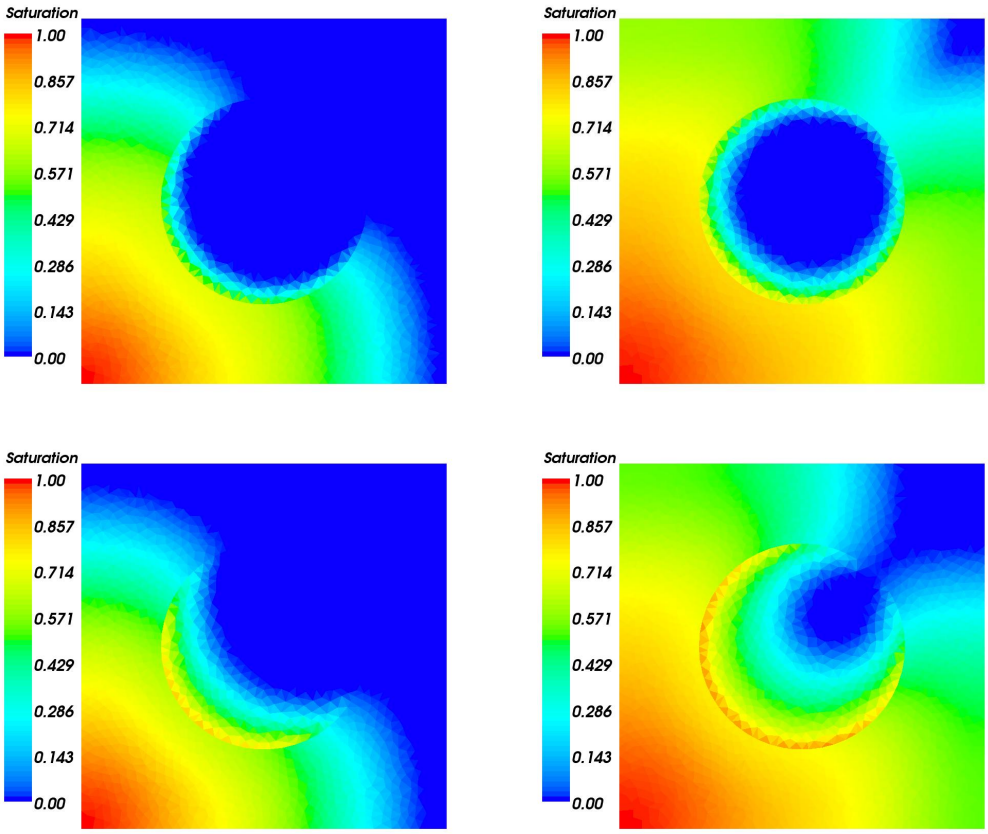

FIGURE 10. Example of solution fields from example 2. Top row: Homogeneous capillary pressure. Bottom row: Heterogeneous capillary pressure. Left column: $t = 1.0$. Right column: $t = 2.0$.

equal to 1), which is otherwise filled with oil. A corresponding sink (with source strength equal to -1) is placed at the upper right corner.

Numerical computations (with the triangulation shown in 7 (right)) are again performed using both a capillary homogeneous (k is put to 1 in equation (57)) and capillary heterogeneous domain. Results are presented in Figure 10 for two different simulation times.

Again we observe the significant difference in flow behavior between the two cases. The case with homogeneous capillary pressure displays a smooth solution field very much influenced by the low permeable circular inclusion, and in particular obtain an earlier water breakthrough than the case with heterogeneous capillary pressure. In the latter case saturation discontinuites are formed at the boundaries of the circular inclusion, and moreover, the circular inclusion is again much more penetrated by water, thus leading to a later water breakthrough. Obviously, such effects can be even more important when simulating complex real reservoirs.

8. Conclusions

The present paper concerns two-phase flow in porous media with heterogeneous capillary pressure functions. This problem has received very little attention in the literature, despite its importance in real flow situations. Moreover, the problem also constitutes a challenge for numerical discretizations, since saturation discontinuities arise at the interface between the different homogeneous regions in the domain.

Examining a one-dimensional model problem, for which a semi-analytical solution is known, it is found that a standard scheme based on harmonic averaging of the absolute permeability, and which possesses the important property of being pressure continuous at the discrete level, gives the best numerical results. A recent two-dimensional multi point flux approximation scheme, which is also pressure continuous at the discrete level, is then extended to account for two-phase flow, such that we obtain a robust an accurate discretization of the two-phase flow pressure equation. We solve the two-phase flow model in an implicit pressure explicit saturation setting, using a recent fractional flow formulation, which is well suited for capillary pressure heterogeneity. The corresponding saturation equation is discretizized by a second-order central upwind scheme.

We present a few numerical examples in order to illustrate the significance of capillary pressure heterogeneity in two-dimensional two-phase flow, using both structured quadrilateral and unstructured triangular grids. It is i.a. found that capillary heterogeneity can have a significant effect on water breakthrough. Thus it should be reasonable to expect that capillary pressure heterogeneities can have an even more pronounced effect in complex real reservoirs, which further emphasizes the importance of an accurate and reliable numerical treatment of these rather involved nonlinear problems.

Acknowledgements

The Research Council of Norway under grant numbers 163316/S30, 166513/V30 ("SAGA-GEO") and 197739/V30 ("DMPL"), ConocoPhilips, DNO and StatoilHydro are gratefully acknowledged for their financial support. The research of the second author has also been supported by A/S Norske Shell. We also thank J. R. Shewchuk for permission to use the Triangle software for generation of the unstructured grids (http://www-2.cs.cmu.edu/~quake/triangle.html).

References

[1] T. Arbogast, M. F. Wheeler and I. Yotov, Mixed finite elements for elliptic problems with tensor coefficients as cell centered finite differences. *SIAM J. Numer. Anal.*, 34(2): 828-852, 1997.

[2] T. Arbogast, C. N. Dawson, P.T. Keenan, M. F. Wheeler and I. Yotov, Enhanced cell-centered finite differences for elliptic equations on general geometry. *SIAM J. Sci. Comput.*, 19(2): 404-425, 1998.

[3] P. Arminjon, M. C. Viallon and A. Madrane, A finite volume extension of the Lax-Friedrichs and Nessyahn-Tadmor schemes for conservation laws on unstructured grids. *Int. J. Comput. Fluid Dyn.*, 9(1): 1-22, 1997.

[4] K. Aziz and A. Settari, *Petroleum Reservoir Simulation*, Elsevier Applied Science Publishers, 1979.

[5] I. Aavatsmark, T. Barkve, Ø. Bøe and T. Mannseth, Discretization on Unstructured Grids for Inhomogenous, Anisotropic Media. Part I: Derivation of the Methods. *SIAM J. Sci. Comput.*, 19(5): 1700-1716, 1998.

[6] I. Aavatsmark, An introduction to multi point flux approximations for quadrilateral grids. *Comput. Geosci.*, 6(3-4): 405-432, 2002.

[7] F. Brezzi, and M. Fortin, Mixed and Hybrid Finite Elements Methods. *Springer Series in Computational Mathematics 15, Springer-Verlag*, 1991.

[8] S. Bryson and D. Levy, Balanced central schemes for the shallow water equations on unstructured grids. *SIAM J. Sci. Comput.*, 27(2), pp. 532-552, 2005.

[9] Z. Cai, J. E. Jones, S. F. McCormick and T. F. Russell, Control-volume mixed finite element methods. *Comput. Geosci.*, 1: 289-315, 1997.

[10] Z. Chen, G. Huan and B. Li, An improved IMPES method for two-phase flow in porous media. *Transp. in Porous Media*, 54 (3), pp. 361-376, 2004.

[11] M. G. Edwards and C. F. Rogers, Finite volume discretization with imposed flux continuity for the general tensor pressure equations. *Comput. Geosci.*, 2, pp. 259-290, 1998.

[12] M. G. Edwards, Unstructured, control-volume distributed, full-tensor finite-volume schemes with flow based grids. *Comput. Geosci.*, 6, pp. 433-452, 2002.

[13] M. G. Edwards and H. Zheng, A quasi-positive family of continuous Darcy-flux finite volume schemes with full pressure support. *J. Comput. Phys.*, 227, pp. 9333-9364, 2008.

[14] M. G. Edwards and H. Zheng, Double families of quasi-positive darcy-flux approximations with highly anisotropic tensors on structured and unstructured grids. *J. Comput. Phys.*, 229, pp. 594-625, 2010.

[15] H. A. Friis, M. G. Edwards and J. Mykkeltveit, Symmetric positive definite flux-continuous full-tensor finite-volume schemes on unstructured cell centered triangular grids. *SIAM J. Sci. Comput.*, 31(2), pp. 1192-1220, 2008.

[16] H. A. Friis and M. G. Edwards, A family of MPFA finite-volume schemes with full pressure support for the general tensor pressure equation on cell-centered triangular grids. *J. Comput. Phys.*, 230(1), pp. 205-231, 2011.

[17] H. A. Friis, M. G. Edwards and P. A. Tyvand, Flux-continuous finite-volume approximations for the time-dependent diffusion equation. *Submitted*, 2011.

[18] F. Hermeline, Approximation of 2-D and 3-D diffusion operators with variable full tensor coefficients on arbitrary meshes. *Computer Meth. Appl. Mech. Engng.*, 196, pp. 2497-2526, 2007.
[19] H. Hoteit and A. Firoozabadi, Numerical modeling of two-phase flow in heterogeneous permeable media with different capillarity pressures. *Adv. Water Resources*, 31, pp. 56-73, 2008.
[20] J. Hyman, M. Shashkov and S. Steinberg, The numerical solution of diffusion problems in strongly heterogeneous non-isotropic materials. *J. Comput. Phys.*, 132, pp. 130-148, 1997.
[21] A. Kurganov and E. Tadmor, New high-resolution central schemes for nonlinear conservation laws and convection-diffusion equations. *J. Comput. Phys.*, 160 (1), pp. 241-282, 2000.
[22] A. Kurganov, S. Noelle and G. Petrova, Semidiscrete central-upwind schemes for hyperbolic conservation laws and Hamiliton-Jacobi equations. *SIAM J. Sci. Comput.*, 23 (3), pp. 707-740, 2001.
[23] A. Kurganov and G. Petrova, Central-upwind schemes on triangular grids for hyperbolic systems of conservation laws. *Numer. Methods Partial Differential Eq.*, 21, pp. 536-552, 2005.
[24] J. Niessner, R. Helmig, H. Jakobs and J. E. Roberts, Interface condition and linearization schemes in the Newtion iterations for two-phase flow in heterogeneous porous media. *Adv. Water Resources*, 28, pp. 671-687, 2005.
[25] M. Pal, M. G. Edwards and A. R. Lamb, Convergence study of a family of flux continuous, finite volume schemes for the general tensor pressure equation. *Int. J. Numer. Meth. Fluids*, 51, pp. 1177-1203, 2006.
[26] C. J. van Duijn and M. J. de Neef, Similarity solution for capillary redistribution of two phases in a porous medium with a single discontinuity. *Adv. Water Resources*, 21, pp. 451-461, 1998.
[27] Y. Yortsos and J. Chang, Capillary effects in steady-state flow in heterogeneous cores. *Tranp. in Porous Media*, 5, pp. 399-420, 1990.